A Modified Strain Gradient Beam Constraint Model

Mohammad Arhami[1], Hamid Moeenfard[1,2*]

[1] School of Mechanical Engineering, Ferdowsi University of Mashhad, Mashhad, Khorasan Razavi, Iran

[2] Center of Excellence in Soft Computing and Intelligent Information Processing (SCIIP), Ferdowsi University of Mashhad, Mashhad, Khorasan Razavi, Iran

Corresponding author's email: h_moeenfard@um.ac.ir

Abstract

The objective of this paper is to develop a modified strain gradient beam constraint model (MSGBCM) to improve modeling accuracy of small-scale compliant mechanisms. First, a simple nano/micro flexure beam under the effect of end loads is considered. The virtual work principle is employed to formulate the load-displacement behavior of the system based on the modified strain gradient theory. It is observed that as the size of the structure becomes smaller, the elements of the elastic stiffness and load stiffening matrices severely deviate from their corresponded values in the beam constraint model (BCM). Then, a closed-form expression is proposed for the nonlinear strain energy of the nano/micro flexure beams in terms of their tip displacements. This energy expression is then utilized to model load-displacement relationship of micron/submicron size parallelogram (P) flexures. Moreover, analytical formulas are derived for the axial, transverse and rotational stiffnesses of P-flexures. The most important observation is that the axial stiffness loss of small-scale P-flexures resulted from the movement of the stage in the transverse direction, may be seriously overestimated by the BCM. The MSGBCM developed in this paper can be easily

extended for investigating static and dynamic behavior of more complex micron and submicron size flexure units.

Keywords:

Beam flexure, Beam constraint model, Modified strain gradient elasticity theory, Modified strain gradient beam constraint model, Parallelogram flexure.

1- Introduction

Mechanisms are used to transform an input force or movement into desired outputs. Classical mechanisms usually include different rigid members sliding on, or rotating around each other with the ultimate aim of providing desired motion in the mechanisms output. The performance of the classical mechanisms is negatively affected by wear, backlash and friction [1, 2]. Moreover, fabrication of prismatic and revolute joints which are essential parts of the classical mechanisms are very difficult (if not impossible) in nano and micro dimensions. To avoid these shortcomings, compliant mechanisms are becoming widely popular. These mechanisms provide motion guidance via elastic deformation of their constitutive beams. Due to their monolithic structure, they don't require assembly or lubrication. They are especially suited for micron size apparatuses which require high precision and large motion range. Among such applications, one can point to the micro-grippers [3-5], micro/nano manipulators [6-8], displacement amplification mechanisms [9], force, displacement and acceleration sensors [10-12], compact and affordable motion stages for semiconductor wafer inspection [13] and micro scanners in high-speed imaging [14].

Compliant mechanisms are usually designed for achieving large motion ranges. This is achieved by the large deflection of the constitutive beams which on the other hand, activates the geometric nonlinearities in the system. Consequently, an accurate model of these mechanisms shall

take the geometric nonlinearities into account. Large deflection behavior of thin beams under the effect of different applied loads have been well-studied in previous studies [15-21]. Among different models and strategies, the beam constraint model (BCM) developed by Awtar and Sen [22] is best suited for intermediate/large deflection analysis of beams in compliant mechanisms. The advantages of BCM are as follows:

1- It provides sufficiently accurate expressions for the load-displacement behavior of the beam. This is especially important from a design perspective in which the designer is interested in modeling the static or dynamic behavior of the motion stage.

2- It suggests an acceptable tradeoff between the complexity of the solution procedure and accuracy of the results.

3- Using BCM, the nonlinear strain energy of a cantilever flexure beam can be easily expressed in terms of its tip displacements. This specification makes it quite easy to extend the applicability of BCM from a simple beam flexure to more complex flexure modules such as parallelogram (P) [22-25], double parallelogram (DP) [26, 27] and paired double parallelogram (DP-DP) [27, 28] flexures.

The strain energy expressions developed by BCM is not only useful for static analysis of complex flexures, but also it provides a comfortable platform for their dynamic modeling. For example, Cui et al [29] used the constrained equations resulted from BCM to present a lumped parameter model for a structure with multiple DP flexure modules. The transfer function of their dynamic model was used to identify complex nonminimum phase zeros of the system. Findings of this research were later experimentally verified for a desktop size flexure [30].

One of the most important superiorities of the compliant mechanisms over their traditional counterparts is their applicability in small scale devices. In fact, fabrication of traditional mechanisms in nano or micro dimensions is very difficult. So, for providing constrained motion guidance in these dimensions, employing compliant mechanisms may be the only available option. As instances of micron size flexures, one can point to the works of Awtar and co-workers in which they demonstrated novel double parallelogram–tilted-beam double parallelogram (DP-TDP) [31], clamped paired double parallelogram (C-DP-DP) [32] and XY [33] flexure mechanisms that enabled large stroke in electrostatic comb-drive actuators. In all these works, the theoretical findings were based on a classical elasticity theory. On the other hand, it has been shown in many other studies (see [34-37] as a few examples) that classical elasticity theory fails in prediction of the material behavior in micro or nano dimensions. To overcome these limitations, several size dependent theories were presented. Among them, one can mention the micropolar theory [38-40], nonlocal theory of Eringen [41], modified strain gradient [34] and modified couple stress [42] theories which were propose to fill the gap between the experimental observations and theoretical findings. Micropolar elasticity utilizes some extra rotational degrees of freedom at each material point to improve modeling accuracy [43]. Nonlocal elasticity theory developed by Eringen [44, 45] is based on the assumption that the stress at a point is a function of strains at all points in the continuum. To simplify the corresponded mathematical formulation of the micropolar theory, researchers proposed several other size dependent theories such as modified strain gradient (MSG) [34] and modified couple stress (MCS) [42] theories. By including three non-classical material constants in the derivations, Lam et al [34] proposed the MSG formulation. The MCS theory presented by Yang et al [42] added one non-classical as well as two classical material constants to the constitutive equations of elastic materials. It has to be noted that the use of MSG theory in mathematical formulation of mechanical structures using energy-based techniques, is simpler than

those of the micropolar and nonlocal theories. Moreover, MSG theory is more general than MCS one. In fact, the MCS theory can be obtained by removing two non-classical material constants from the MSG formulation [46].

Static and dynamic behavior of microbeams based on size dependent theories have been well-investigated in previous studies. For example, Vatankhah and Kahrobaiyan [47] Investigated the size-dependency in free-vibration of micro-resonators based on the strain gradient theory. Kong et al [48] solved the static and dynamic problem of Euler-Bernoulli beams on the basis of MSG theory. They found that when the thickness of the beam becomes comparable to the material length scale parameter, beam deflection decreases and natural frequencies increase remarkably. Wang et al [49] investigated the same problem for the small Timoshenko beams and concluded that when the beam thickness is comparable to the material length scale parameter, results of a strain gradient elasticity theory substantially differs from those of classical theories. Radgolchin and Moeenfard [50] utilized the MSG along with the random vibration theory to statistically model the harvested power in micron size energy harvesters. The strain gradient theory has also been utilized for modeling nonlinear large deflection behavior of beams. In a leading publication, Kahrobaiyan et al [51] developed a nonlinear size dependent Euler-Bernoulli beam model. Rahaeifard et al [52] studied the deflection and static pull-in of microbridges based on the MCS theory. The bucking analysis of micron and sub-micron size beams were carried out in [53] and [54] by employing strain gradient theory. The nonlinear MSG theory was used in [46] to analyze the vibrational behavior of electrostatically actuated shear deformable microarches.

As reviewed, size dependent theories have been extensively utilized to model the static and dynamic behavior of nano and micro beams. However, as far as the authors know, these theories have not been yet employed to modify the BCM which is widely applicable for analysis of

compliant mechanisms. So, the current paper aims to develop a novel method called *modified strain gradient beam constrain model (MSGBCM)* to enable accurate analysis of nano or micro scale flexures. The principle of virtual work is utilized to formulate the problem for a strain gradient beam flexure. Then closed-from analytic expressions are derived for the nonlinear strain energy of the beam which is further employed for modeling load-displacement behavior of nano and micro scale P-flexures. Extensive parametric studies are also performed to characterize the length scale effects on behavior of flexure beams as well as P-flexures. The core finding of this research is that for accurate analysis of small size flexures, the length scale effects shall be taken into account.

2- Problem formulation

A thin microbeam as shown in Fig. 1 is considered. The length, width and thickness of this beam is assumed to be L, b and h respectively. The microbeam deflects under the effects of end forces F_Z and F_X as well as end moment M_Y.

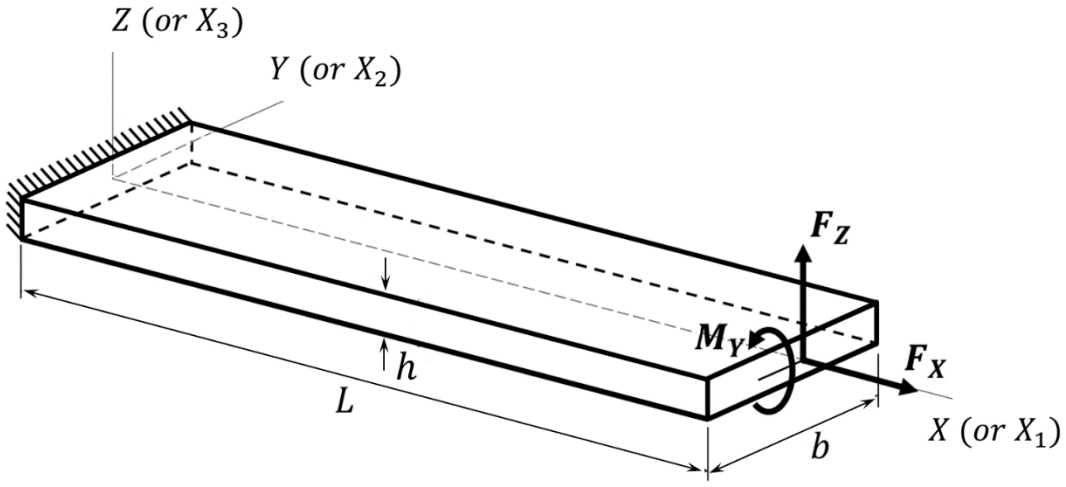

Fig. 1: Schematic view of the thin nano/microbeam under study

Based on the thin beam theory, the displacement vector of an arbitrary element placed at a distance Z from the neutral axis of the beam can be obtained as [55]

$$\vec{\mathcal{U}} = \begin{Bmatrix} \mathcal{U}_1(X,Z) \\ \mathcal{U}_2(X,Z) \\ \mathcal{U}_3(X,Z) \end{Bmatrix} = \begin{Bmatrix} U(X) \\ 0 \\ W(X) \end{Bmatrix} - Z \begin{Bmatrix} \frac{dW(X)}{dX} \\ 0 \\ 0 \end{Bmatrix} \tag{1}$$

In this equation, $\mathcal{U}_1$, $\mathcal{U}_2$ and $\mathcal{U}_3$ are the displacements along the X, Y and Z axes respectively. Moreover, $U(X)$ is the axial displacement of the neutral axis and $W(X)$ is its transverse deflection. Using the von-Karman strain [56] along with employing Eq. (1), the only nonzero element of the strain tensor is derived as

$$\varepsilon_{11}(X) = \frac{\partial \mathcal{U}_1(X,Z)}{\partial X} + \frac{1}{2}\left(\frac{\partial \mathcal{U}_3(X,Z)}{\partial Z}\right)^2 = \frac{dU(X)}{dX} + \frac{1}{2}\left(\frac{dW(X)}{dX}\right)^2 - Z\frac{d^2W(X)}{dX} \tag{2}$$

Using Eq. (1), the infinitesimal rotation vector $\vec{\Theta} = \frac{1}{2}\text{curl}\left(\vec{\mathcal{U}}\right)$ [51] is obtained as

$$\vec{\Theta} = -\begin{Bmatrix} 0 \\ \frac{dW(X)}{dX} \\ 0 \end{Bmatrix} \tag{3}$$

Now, Eq. (3) can be utilized to obtain the symmetric part of the rotation gradient tensor $\chi_{ij}^s = \left(\Theta_{i,j} + \Theta_{j,i}\right)/2$ [51]. The nonzero elements of this tensor are as

$$\chi_{12}^s = \chi_{21}^s = -\frac{1}{2}\frac{d^2W(X)}{dX^2} \tag{4}$$

The strain tensor ε can be used to find the elements of the dilatation gradient vector $\gamma_i = \varepsilon_{mm,i}$ [43] as

$$\gamma_1 = \frac{d^2U(X)}{dX^2} + \frac{dW(X)}{dX}\frac{d^2W(X)}{dX^2} - Z\frac{d^3W(X)}{dX^3} \tag{5}$$

$$\gamma_2 = 0 \tag{6}$$

$$\gamma_3 = -\frac{d^2W(X)}{dX^2} \tag{7}$$

The deviatoric stretch gradient tensor $\eta_{ijk}^{(1)}$ can also be derived using [57]

$$\eta_{ijk}^{(1)} = -\frac{1}{15}\left[\delta_{ij}\left(\varepsilon_{mm,k} + 2\varepsilon_{mk,m}\right) + \delta_{jk}\left(\varepsilon_{mm,i} + 2\varepsilon_{mi,m}\right) + \delta_{ki}\left(\varepsilon_{mm,j} + 2\varepsilon_{mj,m}\right)\right] + \frac{1}{3}\left(\varepsilon_{jk,i} + \varepsilon_{ki,j} + \varepsilon_{ij,k}\right) \tag{8}$$

in which δ is the Kronecker delta. By substituting ε from Eq.(2) into Eq.(8) the nonzero elements of this tensor are obtained as

$$\eta_{111}^{(1)} = \frac{2}{5}\left(\frac{d}{dX}\left(\frac{dU(X)}{dX} + \frac{1}{2}\left(\frac{dW(X)}{dX}\right)^2\right) - Z\frac{d^3W(X)}{dX^3}\right) \tag{9}$$

$$\eta_{113}^{(1)} = \eta_{311}^{(1)} = \eta_{131}^{(1)} = -\frac{4}{15}\frac{d^2W(X)}{dX^2} \tag{10}$$

$$\eta_{122}^{(1)} = \eta_{133}^{(1)} = \eta_{212}^{(1)} = \eta_{221}^{(1)} = \eta_{313}^{(1)} = \eta_{331}^{(1)} = -\frac{1}{5}\left(\frac{d}{dX}\left(\frac{dU(X)}{dX} + \frac{1}{2}\left(\frac{dW(X)}{dX}\right)^2\right) - Z\frac{d^3W(X)}{dX^3}\right) \tag{11}$$

$$\eta_{223}^{(1)} = \eta_{232}^{(1)} = \eta_{322}^{(1)} = \frac{1}{15}\frac{d^2W(X)}{dX^2} \tag{12}$$

$$\eta_{333}^{(1)} = \frac{1}{5}\frac{d^2W(X)}{dX^2} \tag{13}$$

Now, the nonzero elements of the stress tensor $\sigma_{ij} = \lambda \mathrm{tr}(\varepsilon)\delta_{ij} + 2\mu\varepsilon_{ij}$ as well as higher order stresses $p_i = 2\mu l_0^2 \gamma_i$, $\tau_{ijk}^{(1)} = 2\mu l_1^2 \eta_{ijk}^{(1)}$ and $m_{ij}^s = 2\mu l_2^2 \chi_{ij}^s$ are calculated by [51]

$$\sigma_{11} = E\left(\frac{dU(X)}{dX} + \frac{1}{2}\left(\frac{dW(X)}{dX}\right)^2 - Z\frac{d^2W(X)}{dX^2}\right) \tag{14}$$

$$p_1 = 2\mu l_0^2\left(\frac{d}{dX}\left(\frac{dU(X)}{dX} + \frac{1}{2}\left(\frac{dW(X)}{dX}\right)^2\right) - Z\frac{d^3W(X)}{dX^3}\right) \tag{15}$$

$$p_3 = -2\mu l_0^2\frac{d^2W(X)}{dX^2} \tag{16}$$

$$\tau_{111}^{(1)} = \frac{4}{5}\mu l_1^2\left(\frac{d^2U(X)}{dX^2} - Z\frac{d^3W(X)}{dX^3} + \frac{d^2W(X)}{dX^2}\right) \tag{17}$$

$$\tau_{113}^{(1)} = \tau_{311}^{(1)} = \tau_{131}^{(1)} = -\frac{8}{15}\mu l_1^2\frac{d^2W(X)}{dX^2} \tag{18}$$

$$\tau_{122}^{(1)} = \tau_{133}^{(1)} = \tau_{212}^{(1)} = \tau_{221}^{(1)} = \tau_{313}^{(1)} = \tau_{331}^{(1)}$$
$$= -\frac{2}{5}\mu l_1^2\left(\frac{d}{dX}\left(\frac{dU(X)}{dX} + \frac{1}{2}\left(\frac{dW(X)}{dX}\right)^2\right) - Z\frac{d^3W(X)}{dX^3}\right) \tag{19}$$

$$\tau_{223}^{(1)} = \tau_{232}^{(1)} = \tau_{322}^{(1)} = \frac{2}{15}\mu l_1^2\frac{d^2W(X)}{dX^2} \tag{20}$$

$$\tau_{333}^{(1)} = \frac{2}{5}\mu l_1^2\frac{d^2W(X)}{dX^2} \tag{21}$$

$$m_{12} = m_{21} = -\mu l_2^2\frac{d^2W(X)}{dX^2} \tag{22}$$

in which E is the Young's modulus of elasticity, l_0, l_1 and l_2 are the length scale parameters and λ and μ are Lamé constants and are obtained using [58]

$$\lambda = \frac{vE}{(1+v)(1-2v)} \tag{23}$$

$$\mu = \frac{E}{2(1+v)} \tag{24}$$

In Eqs. (23) and (24), v denotes the Poison's ratio.

Finally, by substituting Eqs. (2), (4)-(7) and (9)-(22) into the potential energy expression $V = \frac{1}{2}\int_0^L \int_A \left(\sigma_{ij}\varepsilon_{ij} + p_i\gamma_i + \tau_{ijk}^{(1)}\eta_{ijk}^{(1)} + m_{ij}^s\chi_{ij}^s\right)dAdx$ [34], the strain energy of the beam is simply derived in terms of the displacement field as

$$V = \frac{1}{2}\int_0^L \int_A \left\{ E\left(\frac{dU(X)}{dX} + \frac{1}{2}\left(\frac{dW(X)}{dX}\right)^2 - Z\frac{d^2W(X)}{dX^2}\right)^2 + \mu\left(2l_0^2 + \frac{8}{15}l_1^2 + l_2^2\right)\left(\frac{d^2W(X)}{dX^2}\right)^2 \right.$$
$$\left. + 2\mu\left(l_0^2 + \frac{2}{5}l_1^2\right)\left(\frac{d}{dx}\left(\frac{dU(X)}{dX} + \frac{1}{2}\left(\frac{dW(X)}{dX}\right)^2\right) - Z\frac{d^3W(X)}{dX^3}\right)^2 \right\} dAdx \tag{25}$$

where A is the area cross section of the beam. By defining $\varepsilon_0(X) = dU(X)/dX + (dW(X)/dX)^2/2$ as the axial strain of the neutral axis and performing the inner integral, the strain energy expression is simplified as

$$V = \frac{1}{2}\int_0^L \left\{ k_1\varepsilon_0^2(X) + k_2\left(\frac{d\varepsilon_0(X)}{dX}\right)^2 + k_3\left(\frac{d^2W(X)}{dX^2}\right)^2 + k_4\left(\frac{d^3W(X)}{dX^3}\right)^2 \right\} dX \tag{26}$$

In this equation, the parameters k_1, k_2, k_3 and k_4 are defined by

$$k_1 = EA$$
$$k_2 = 2\mu A\left(l_0^2 + \frac{2}{5}l_1^2\right)$$
$$k_3 = EI + \mu A\left(2l_0^2 + \frac{8}{15}l_1^2 + l_2^2\right)$$
$$k_4 = 2\mu I\left(l_0^2 + \frac{2}{5}l_1^2\right) \tag{27}$$

where I is the second area moment of inertia of the cross section around the neutral axis.

Applying the variation operator $\tilde{\delta}$ on both sides of Eq. (26) leads to

$$\tilde{\delta}V = \int_0^L \left\{ k_1 \varepsilon_0(X) \tilde{\delta}\varepsilon_0(X) + k_2 \frac{d\varepsilon_0(X)}{dX} \tilde{\delta}\left(\frac{d\varepsilon_0(X)}{dX}\right) + k_3 \frac{d^2W(X)}{dX^2} \tilde{\delta}\left(\frac{d^2W(X)}{dX^2}\right) + k_4 \frac{d^3W(X)}{dX^3} \tilde{\delta}\left(\frac{d^3W(X)}{dX^3}\right) \right\} dX \tag{28}$$

By twice performing the integration by parts and noting that $\tilde{\delta}\varepsilon_0 = \tilde{\delta}(dU/dX) + (dW/dX)\tilde{\delta}(dW/dX)$, Eq. (28) can be re-expressed as

$$\begin{aligned} \tilde{\delta}V = & \int_0^L \left\{ \frac{d}{dX}\left(\left(-k_1\varepsilon_0 + k_2 \frac{d^2\varepsilon_0}{dX^2} \right) \frac{dW}{dX} \right) + k_3 \frac{d^4W}{dX^4} - k_4 \frac{d^6W}{dX^6} \right\} \tilde{\delta}W dX \\ & - \int_0^L \frac{d}{dX}\left(k_1\varepsilon_0 - k_2 \frac{d^2\varepsilon_0}{dX^2} \right) \tilde{\delta}U dX + \left[\left(k_1\varepsilon_0 - k_2 \frac{d^2\varepsilon_0}{dX^2} \right) \tilde{\delta}U \right]_{X=0}^{X=L} \\ & + \left[k_2 \frac{d\varepsilon_0}{dX} \tilde{\delta}\left(\frac{dU}{dX}\right) \right]_{X=0}^{X=L} + \left[k_4 \frac{d^3W}{dX^3} \tilde{\delta}\left(\frac{d^2W}{dX^2}\right) \right]_{X=0}^{X=L} \\ & + \left[\left(\left(k_1\varepsilon_0 - k_2 \frac{d^2\varepsilon_0}{dX^2} \right) \frac{dW}{dX} - k_3 \frac{d^3W}{dX^3} + k_4 \frac{d^5W}{dX^5} \right) \tilde{\delta}W \right]_{X=0}^{X=L} \\ & + \left[\left(k_2 \frac{d\varepsilon_0}{dX} \frac{dW}{dX} + k_3 \frac{d^2W}{dX^2} - k_4 \frac{d^4W}{dX^4} \right) \tilde{\delta}\left(\frac{dW}{dX}\right) \right]_{X=0}^{X=L} \end{aligned} \tag{29}$$

On the other hand, based on the principle of virtual work [23], one can say

$$\tilde{\delta}V = F_X \tilde{\delta}U_{tip} + F_Z \tilde{\delta}W_{tip} + M_Y \tilde{\delta}\theta_{tip} \tag{30}$$

By comparing (29) and (30) , the governing equations of the system and the corresponded boundary conditions can be obtained. To express these equations more conveniently, the following normalized variables are defined.

$$x = \frac{X}{L}, \;\; u(x) = \frac{U(X)}{L}, \;\; w(x) = \frac{W(X)}{L}, \;\; f_x = \frac{F_X L^2}{EI}, \;\; f_z = \frac{F_Z L^2}{EI}, \;\; m_y = \frac{M_Y L}{EI} \tag{31}$$

Using these normalized variables, after some mathematical simplifications, the governing equations of the strain gradient beam are derived as

$$\left(\varepsilon_0(x) - \frac{a_2}{a_1}\varepsilon_0''(x)\right)' = 0 \tag{32}$$

$$a_4 w^{(6)}(x) - a_3 w^{(4)}(x) + f_x w''(x) = 0 \tag{33}$$

In these equations, the prime denotes differentiation with respect to x. Moreover, the parameters a_i $(i = 1, 2, 3, 4)$ in these equations are defined by

$$a_1 = 12\left(\frac{L}{h}\right)^2$$

$$a_2 = \frac{12}{(1+\nu)h^2}\left(l_0^2 + \frac{2}{5}l_1^2\right)$$

$$a_3 = 1 + \frac{6}{(1+\nu)h^2}\left(2l_0^2 + \frac{8}{15}l_1^2 + l_2^2\right)$$

$$a_4 = \frac{1}{(1+\nu)L^2}\left(l_0^2 + \frac{2}{5}l_1^2\right) \tag{34}$$

The normalized classical and nonclassical boundary conditions of the system are also derived as

$$\varepsilon_0'(0) = \varepsilon_0'(1) = 0 \tag{35}$$

$$\varepsilon_0(1) - \frac{a_2}{a_1}\varepsilon_0''(1) = \frac{f_x}{a_1} \tag{36}$$

$$w(0) = w'(0) = w''(0) = w'''(1) = 0 \tag{37}$$

$$a_4 w^{(5)}(1) - a_3 w'''(1) + f_x w'(1) = f_Z \tag{38}$$

$$a_3 w''(1) - a_4 w^{(4)}(1) = m_y \tag{39}$$

3- Modified strain gradient BCM

In this section, the MSGBCM will be developed and applied to derive a strain energy expression for a flexure nano/microbeam in terms of its end displacements. To do so, we proceed by integrating Eq. (32) from x to 1 which by considering boundary condition (36) leads to

$$\varepsilon_0(x) - \frac{a_2}{a_1}\varepsilon_0''(x) = \frac{f_x}{a_1} \tag{40}$$

Now, by utilizing boundary condition (35) the solution of differential equation (40) is derived as

$$\varepsilon_0(x) = u'(x) + \frac{1}{2}w'^2(x) = \frac{f_x}{a_1} \tag{41}$$

This equation implies that the axial strain of the neutral axis is constant along the beam length. By integrating both sides of the second equality in (41) from 0 to 1 while noting that $u(0) = 0$ and $u(1) = u_{tip}$, one can conclude

$$u_{tip} = \frac{f_x}{a_1} - \frac{1}{2}\int_0^1 w'^2(x)dx \tag{42}$$

The first term in this equation is the results of elastic stretching of the microbeam resulted from the axial tip load, while the second term is the consequence of the kinematic constraint which relates the tip axial displacement to the transverse deflection. This equation will be employed later to investigate the elastokinematic effects in the axial direction.

To capture the effect of axial force f_x on the beam's deflection, the transverse deflection of the beam is perturbed using f_x as the perturbation parameter as

$$w(x) = \sum_{i=0}^{2} w_i(x) f_x^i + O(f_x^3) \tag{43}$$

By substituting Eq. (43) into Eq. (33) and equating the like powers of f_x equal to zero, the following boundary value differential equations are obtained.

$$O(f_x^0): \quad a_4 w_0^{(6)}(x) - a_3 w_0^{(4)}(x) = 0 \tag{44}$$

$$O(f_x^1): \quad a_4 w_1^{(6)}(x) - a_3 w_1^{(4)}(x) = -w_0''(x) \tag{45}$$

$$O(f_x^2): \quad a_4 w_2^{(6)}(x) - a_3 w_2^{(4)}(x) = -w_1''(x) \tag{46}$$

Moreover, by considering Eq. (37) and noting that $w(1) = w_{tip}$ and $w'(1) = \theta_{tip}$, the boundary conditions for $w_i(x)$, $i = 0, 1, 2$, are derived as

$$w_i(0) = w_i'(0) = w_i''(0) = 0, \quad i = 0, 1, 2 \tag{47}$$

$$w_0(1) = w_{tip}, \;\; w_0'(1) = \theta_{tip} \tag{48}$$

$$w_i(1) = w_i'(1) = w_j'''(1) = 0, \quad i = 1,2, \quad j = 1, 2, 3 \tag{49}$$

It has to be noted that the natural boundary conditions (38) and (39) will be used later to derive the stiffness matrix of the beam. Anyway, the solution of Eqs. (44)-(46) under the boundary conditions (47)-(49) is derived as a linear combination of w_{tip} and θ_{tip} as

$$w_i(x) = \xi_{1,i}(x) w_{tip} + \xi_{2,i}(x) \theta_{tip}, \quad i = 0, 1, 2 \tag{50}$$

in which $\xi_{j,i}(x)$s are some complicated functions that are presented in appendix I. By substituting Eq. (50) into Eq. (43), the total transverse deflection of the beam is obtained as

$$w(x) = \left(\sum_{i=0}^{2} \xi_{1,i}(x) f_x^i \right) w_{tip} + \left(\sum_{i=0}^{2} \xi_{2,i}(x) f_x^i \right) \theta_{tip} \tag{51}$$

Using Eq. (51) in the natural boundary conditions (38) and (39), it is concluded that

$$\begin{Bmatrix} f_z \\ m_y \end{Bmatrix} = \sum_{i=0}^{2} {f_x}^i \begin{bmatrix} k_{11}^{(i)} & k_{12}^{(i)} \\ k_{21}^{(i)} & k_{22}^{(i)} \end{bmatrix} \begin{Bmatrix} w_{tip} \\ \theta_{tip} \end{Bmatrix} \tag{52}$$

in which all $\left[k^{(i)}\right]$s are independent of f_x. Moreover, in this equation, $\left[k^{(0)}\right]$ is called the elastic stiffness matrix and $\left[k^{(1)}\right]$ and $\left[k^{(2)}\right]$ are the load stiffening matrices. The elements of these matrices can be explicitly expressed in terms of $\xi_{j,i}(x)$s as

$$k_{1,j}^{(0)} = a_4 \xi_{j,0}^{(5)}(1), \quad j = 1,2 \tag{53}$$

$$k_{1,j}^{(i)} = a_4 \xi_{j,i}^{(5)}(1) + \xi'_{j,i-1}(1), \quad i,j = 1,2 \tag{54}$$

$$k_{2,j}^{(i)} = a_3 \xi''_{j,i}(1) - a_4 \xi_{j,i}^{(4)}(1), \quad i = 0,1,2 \ , j = 1,2 \tag{55}$$

Upon substitution of $\xi_{j,i}$s from the appendix I, $k_{i,j}^{(l)}$s can be obtained. Assuming $b_1 = \sqrt{a_3/a_4} > 20$ which is absolutely valid for thin beams, the expressions for $k_{i,j}^{(l)}$ can be greatly simplified using curve fitting technique as

$$k_{ij}^{(0)} = b_2 \left(\hbar_{ij}^{(1)} b_1^2 + \hbar_{ij}^{(2)} b_1 + \hbar_{ij}^{(3)} \right), \quad i,j = 1,2 \tag{56}$$

$$k_{ij}^{(1)} = \frac{\hbar_{ij}^{(4)} b_1 + \hbar_{ij}^{(5)}}{b_1 + \hbar_{ij}^{(6)}}, \qquad i,j = 1,2 \tag{57}$$

$$k_{ij}^{(2)} = \frac{\hbar_{ij}^{(7)}}{b_2 \left(b_1^2 + \hbar_{ij}^{(8)} b_1 + \hbar_{ij}^{(9)} \right)}, \qquad i,j = 1,2 \tag{58}$$

where in these equations, $b_2 = a_4$. The parameters $\hbar_{ij}^{(n)}$ in Eqs. (56)-(58) are some constants and have been presented in Table 1. The maximum error percentage of Eqs. (56)-(58) is less than 0.1%.

Table 1 Numerical values of the parameters $\hbar_{ij}^{(n)}$ appeared in Eqs. (56)-(58)

$\mathcal{k}_{ij}^{(n)}$		(i,j)		
		(1,1)	(1,2)	(2,2)
(n)	(1)	12	-6	4
	(2)	36	-12	4
	(3)	150	-62	29
	(4)	$6/5$	$-1/10$	$2/15$
	(5)	5	$16/15$	$11/10$
	(6)	3	-11	9
	(7)	$-1/700$	$1/1400$	$-11/6300$
	(8)	1	$3/2$	3
	(9)	62	160	74

To obtain the axial constraint kinematic equation, we substitute Eq. (51) into Eq. (42) to obtain

$$u_{tip} = \frac{f_x}{a_1} + \sum_{i=0}^{2} f_x^i \{w_{tip} \quad \theta_{tip}\} \begin{bmatrix} g_{11}^{(i)} & g_{12}^{(i)} \\ g_{21}^{(i)} & g_{22}^{(i)} \end{bmatrix} \begin{Bmatrix} w_{tip} \\ \theta_{tip} \end{Bmatrix} \tag{59}$$

The elements of $\left[g^{(i)}\right]$ are independent of f_x and are functions of $\xi_{j,i}$ as

$$g_{i,j}^{(0)} = -\frac{1}{2}\int_0^1 \left(\xi'_{i,0}\xi'_{j,0}\right) dx\,, \quad i,j = 1,2 \tag{60}$$

$$g_{i,j}^{(1)} = -\frac{1}{2}\int_0^1 \left(\xi'_{i,0}\xi'_{j,1} + \xi'_{j,0}\xi'_{i,1}\right) dx\,, \quad i,j = 1,2 \tag{61}$$

$$g_{i,j}^{(2)} = -\frac{1}{2}\int_0^1 \left(\xi'_{i,1}\xi'_{j,1} + \xi'_{i,0}\xi'_{j,2} + \xi'_{j,0}\xi'_{i,2}\right) dx\,, \quad i,j = 1,2 \tag{62}$$

By substituting $\xi_{j,i}$ from appendix I and performing a curve fitting technique, the elements of $\left[g^{(i)}\right]$s can be accurately expressed in the following compact closed forms with less than 0.1% error.

$$g_{ij}^{(0)} = \frac{\mathscr{g}_{ij}^{(1)} b_1 + \mathscr{g}_{ij}^{(2)}}{b_1 + \mathscr{g}_{ij}^{(3)}}, \quad i = 1,2 \tag{63}$$

$$g_{ij}^{(1)} = \frac{\mathscr{g}_{ij}^{(4)}}{b_2\left(b_1^2 + \mathscr{g}_{ij}^{(5)} b_1 + \mathscr{g}_{ij}^{(6)}\right)}, \quad i = 1,2 \tag{64}$$

$$g_{ij}^{(2)} = \frac{1}{b_2^2\left(\mathscr{g}_{ij}^{(7)} b_1^4 + \mathscr{g}_{ij}^{(8)} b_1^3 + \mathscr{g}_{ij}^{(9)} b_1^2 + \mathscr{g}_{ij}^{(10)} b_1 + \mathscr{g}_{ij}^{(11)}\right)}, \quad i = 1,2 \tag{65}$$

The numerical values of $\mathscr{g}_{ij}^{(n)}$ are as reported in Table 2.

Finally, by substituting ε_0 from Eq. (41) into Eq. (26), the normalized form of the strain energy of the system, $v = V/\mathbb{V}$ (in which $\mathbb{V} = EI/L$) is derived as

$$v = \frac{1}{2}\frac{f_x^2}{a_1} + \frac{1}{2}\int_0^1 \left(a_3 w''^2 + a_4 w'''^2\right) dx \tag{66}$$

Now, by utilizing w from (51), and performing some mathematical manipulations, Eq. (66) can be expressed in the following matrix form.

$$\begin{aligned} v = \frac{1}{2}\{w_{tip} \quad \theta_{tip}\}\begin{bmatrix} v_{11}^{(0)} & v_{12}^{(0)} \\ v_{21}^{(0)} & v_{22}^{(0)} \end{bmatrix}\begin{Bmatrix} w_{tip} \\ \theta_{tip} \end{Bmatrix} + \frac{f_x}{2}\{w_{tip} \quad \theta_{tip}\}\begin{bmatrix} v_{11}^{(1)} & v_{12}^{(1)} \\ v_{21}^{(1)} & v_{22}^{(1)} \end{bmatrix}\begin{Bmatrix} w_{tip} \\ \theta_{tip} \end{Bmatrix} \\ + \frac{f_x^2}{2a_1}\left(1 + a_1\{w_{tip} \quad \theta_{tip}\}\begin{bmatrix} v_{11}^{(2)} & v_{12}^{(2)} \\ v_{21}^{(2)} & v_{22}^{(2)} \end{bmatrix}\begin{Bmatrix} w_{tip} \\ \theta_{tip} \end{Bmatrix}\right) \end{aligned} \tag{67}$$

Table 2 Numerical values of the parameters $\mathscr{g}_{ij}^{(n)}$ appeared in equations (63)-(65)

	$g_{ij}^{(n)}$	(i,j)		
		(1,1)	(1,2)	(2,2)
(n)	(1)	$-3/5$	$1/20$	$-1/15$
	(2)	$-5/2$	$-8/15$	$-11/20$
	(3)	3	-11	9
	(4)	$1/700$	$-1/1400$	$11/6300$
	(5)	1	$3/2$	3
	(6)	62	160	74
	(7)	-4.20×10^4	8.40×10^4	-1.80×10^4
	(8)	-1.30×10^5	4.20×10^5	-9.00×10^4
	(9)	-6.20×10^6	2.20×10^7	-2.00×10^6
	(10)	-1.50×10^7	8.00×10^7	-9.50×10^6
	(11)	-1.50×10^8	3.00×10^9	-3.00×10^3

where the elements of $[v^{(i)}]$ matrices are defined in terms of $\xi_{j,i}$s as

$$v_{i,j}^{(0)} = \int_0^1 \left(a_3 \xi_{i,0}'' \xi_{j,0}'' + a_4 \xi_{i,0}'''' \xi_{j,0}''''\right) dx\,, \quad i,j = 1,2 \tag{68}$$

$$v_{i,j}^{(1)} = \int_0^1 \left(a_3\left(\xi_{i,0}'' \xi_{j,1}'' + \xi_{j,0}'' \xi_{i,1}''\right) + a_4\left(\xi_{i,0}'''' \xi_{j,1}'''' + \xi_{j,0}'''' \xi_{i,1}''''\right)\right) dx\,, \quad i,j = 1,2 \tag{69}$$

$$v_{i,j}^{(2)} = \int_0^1 \left(a_3\left(\xi_{i,1}'' \xi_{j,1}'' + \xi_{i,0}'' \xi_{j,2}'' + \xi_{j,0}'' \xi_{i,2}''\right) + a_4\left(\xi_{i,1}'''' \xi_{j,1}'''' + \xi_{i,0}'''' \xi_{j,2}'''' + \xi_{j,0}'''' \xi_{i,2}''''\right)\right) dx\,, \quad i,j = 1,2 \tag{70}$$

By substituting $\xi_{j,i}$s from appendix I and performing the integrations, the elements of $[v^{(i)}]$s can be easily calculated. By employing curve fitting technique, the expressions for these elements can be expressed in a very compact form as

$$v_{ij}^{(0)} = b_2\left(\nu_{ij}^{(1)} b_1^2 + \nu_{ij}^{(2)} b_1 + \nu_{ij}^{(3)}\right), \quad i,j = 1,2 \tag{71}$$

$$v_{ij}^{(1)} = 0, \quad i,j = 1,2 \tag{72}$$

$$v_{ij}^{(2)} = \frac{\nu_{ij}^{(4)}}{b_2\left(b_1^2 + \nu_{ij}^{(5)} b_1 + \nu_{ij}^{(6)}\right)}, \quad i,j = 1,2 \tag{73}$$

The numerical value of the constants $\nu_{ij}^{(n)}$ are listed in Table 3.

Table 3 Numerical values of the parameters $\nu_{ij}^{(n)}$ appeared in equations (71)-(73)

$\nu_{ij}^{(n)}$	(i,j)		
	(1,1)	(1,2)	(2,2)
(n) (1)	12	−6	4
(2)	36	−12	4
(3)	150	−62	29
(4)	1/700	−1/1400	11/6300
(5)	1	3/2	3
(6)	62	160	74

An investigation of equations (56)-(58), (63)-(65) and (71)-(73) reveals that the following equalities hold between the characteristic matrices $[k]$, $[g]$ and $[v]$. Note that it has already been proven [22] that Eq. (74) is also valid for macro scale beams.

$$\left[v^{(0)}\right] = \left[k^{(0)}\right], \quad \left[g^{(0)}\right] = -\frac{1}{2}\left[k^{(1)}\right], \quad \left[g^{(1)}\right] = \left[v^{(2)}\right] = -\left[k^{(2)}\right] \tag{74}$$

If f_x is small, the terms containing f_x^i $(i \geq 2)$ in (59) can be neglected. Then, this equation can be easily solved for f_x. Using Eq. (74), the corresponded solution can be expressed as

$$f_x = \frac{a_1\left(u_{tip} + \frac{1}{2}\{w_{tip} \quad \theta_{tip}\}\begin{bmatrix} k_{11}^{(1)} & k_{12}^{(1)} \\ k_{21}^{(1)} & k_{22}^{(1)} \end{bmatrix}\begin{Bmatrix} w_{tip} \\ \theta_{tip} \end{Bmatrix}\right)}{\left(1 - a_1\{w_{tip} \quad \theta_{tip}\}\begin{bmatrix} k_{11}^{(2)} & k_{12}^{(2)} \\ k_{21}^{(2)} & k_{22}^{(2)} \end{bmatrix}\begin{Bmatrix} w_{tip} \\ \theta_{tip} \end{Bmatrix}\right)} \tag{75}$$

Now, by substituting Eq. (75) into Eq. (67) and utilizing Eq. (74), the strain energy of the strain gradient beam is simply expressed as

$$v(w_{tip}, \theta_{tip}, u_{tip}) = \frac{1}{2}\{w_{tip} \quad \theta_{tip}\}\begin{bmatrix} k_{11}^{(0)} & k_{12}^{(0)} \\ k_{12}^{(0)} & k_{22}^{(0)} \end{bmatrix}\begin{Bmatrix} w_{tip} \\ \theta_{tip} \end{Bmatrix} + \frac{a_1}{2}\frac{\left(u_{tip} + \frac{1}{2}\{w_{tip} \quad \theta_{tip}\}\begin{bmatrix} k_{11}^{(1)} & k_{12}^{(1)} \\ k_{12}^{(1)} & k_{22}^{(1)} \end{bmatrix}\begin{Bmatrix} w_{tip} \\ \theta_{tip} \end{Bmatrix}\right)^2}{\left(1 - a_1\{w_{tip} \quad \theta_{tip}\}\begin{bmatrix} k_{11}^{(2)} & k_{12}^{(2)} \\ k_{12}^{(2)} & k_{22}^{(2)} \end{bmatrix}\begin{Bmatrix} w_{tip} \\ \theta_{tip} \end{Bmatrix}\right)} \tag{76}$$

The importance of Eq. (76) is that it expresses the strain energy of the strain gradient beam solely in terms of the tip displacements of the nano/microbeam. So, it will be beneficial for obtaining the load-displacement relationships of the system. These equations will be presented briefly in the next section.

By increasing the dimensions of the system and consequently increasing h/l_i , $i = 1,2,3$, the results of the strain gradient formulation shall approach those of the classical BCM. In fact, it can be easily shown that as $h/l_i \to \infty$, the characteristics matrices $[k]$, $[g]$ and $[v]$ resulted from the current formulation tends to the following matrices

$$[k^{(0)}] = \begin{bmatrix} 12 & -6 \\ -6 & 4 \end{bmatrix}, \quad [k^{(1)}] = \begin{bmatrix} \frac{6}{5} & -\frac{1}{10} \\ -\frac{1}{10} & \frac{2}{15} \end{bmatrix}, \quad [k^{(2)}] = \begin{bmatrix} -\frac{1}{700} & \frac{1}{1400} \\ \frac{1}{1400} & -\frac{11}{6300} \end{bmatrix} \tag{77}$$

$$[g^{(0)}] = \begin{bmatrix} -\frac{3}{5} & \frac{1}{20} \\ \frac{1}{20} & -\frac{1}{15} \end{bmatrix},\ [g^{(1)}] = \begin{bmatrix} \frac{1}{700} & -\frac{1}{1400} \\ -\frac{1}{1400} & \frac{11}{6300} \end{bmatrix},\ [g^{(2)}] = \begin{bmatrix} -\frac{1}{42000} & \frac{1}{84000} \\ \frac{1}{84000} & -\frac{1}{18000} \end{bmatrix} \tag{78}$$

$$[v^{(0)}] = \begin{bmatrix} 12 & -6 \\ -6 & 4 \end{bmatrix},\ [v^{(1)}] = \begin{bmatrix} 0 & 0 \\ 0 & 0 \end{bmatrix},\ [v^{(2)}] = \begin{bmatrix} \frac{1}{700} & -\frac{1}{1400} \\ -\frac{1}{1400} & \frac{11}{6300} \end{bmatrix} \tag{79}$$

which are exactly the same as the characteristic matrices reported in [22]. This verifies the accuracy of the proposed formulation. To further study the dependence of the characteristic coefficients $k_{ij}^{(n)}$ to the size of the structure, epoxy beams with characteristics given in Table 4 are considered.

Table 4: Characteristics of the flexure beams under study

Parameter	E	ν	l_0	l_1	l_2	b/h	L/h
Value	1.44	0.38	17.6	17.6	17.6	10	80
Unit	GPa	--	μm	μm	μm	--	--

The variations of the $k_{ij}^{(0)}$, $k_{ij}^{(1)}$ and $k_{ij}^{(2)}$ with h for flexure beams with specifications given in Table 4 have been respectively depicted in Figs. 2-4. It is clear that as the size of the structure is increased, the characteristic coefficients resulted from the strain gradient theory approach their corresponded value obtained by BCM. Moreover, Figs. 2-4 indicate that if the size of the structure is small, the corresponded error resulted from using BCM in predicting the elements of the stiffness matrices can be as large as several hundreds of percent. This is especially true for the stiffness matrix $[k^{(0)}]$ which plays the main role in the nonlinear strain energy expression (please see Eq. (76)).

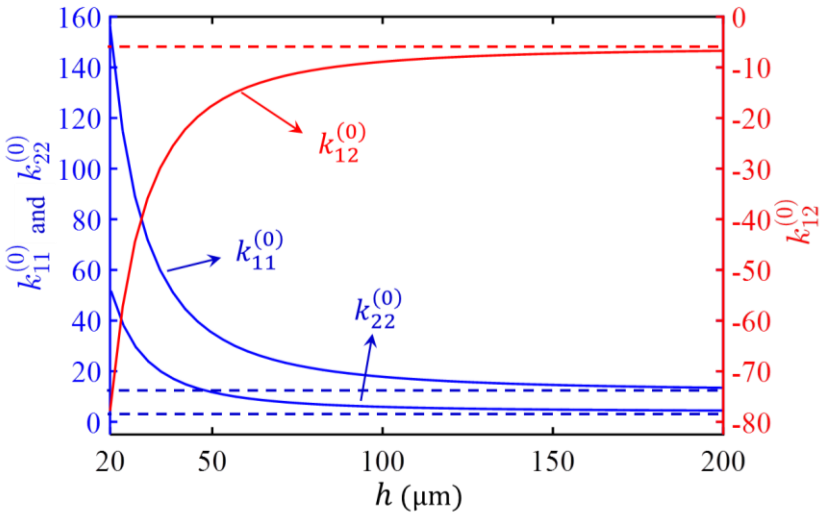

Fig. 2: Variations of the elements of the elastic stiffness matrix $\left[k_{ij}^{(0)}\right]$ of a strain gradient beam with h (dashed asymptotes are the corresponded results of the BCM model)

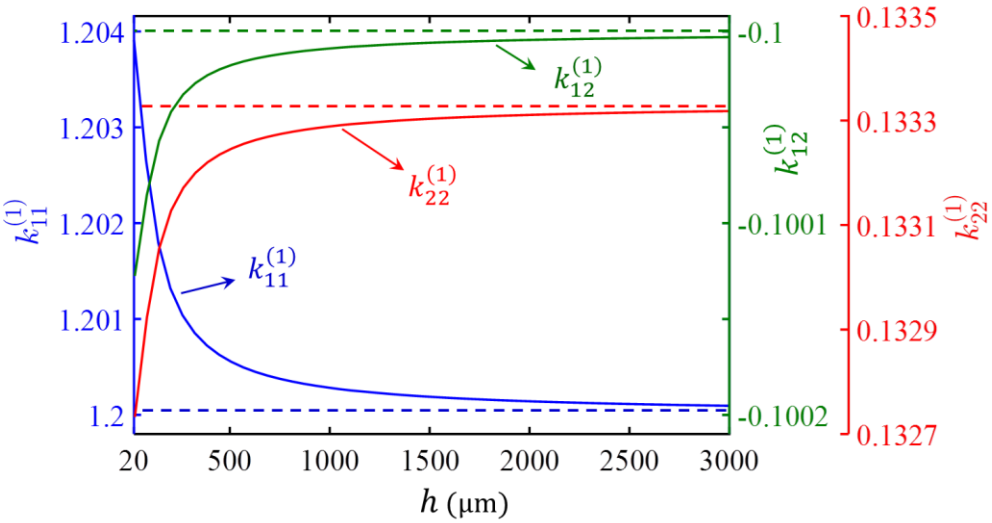

Fig. 3 Variations of the elements of the load stiffening matrix $\left[k_{ij}^{(1)}\right]$ of a strain gradient beam with h (dashed asymptotes are the corresponded results of the BCM model)

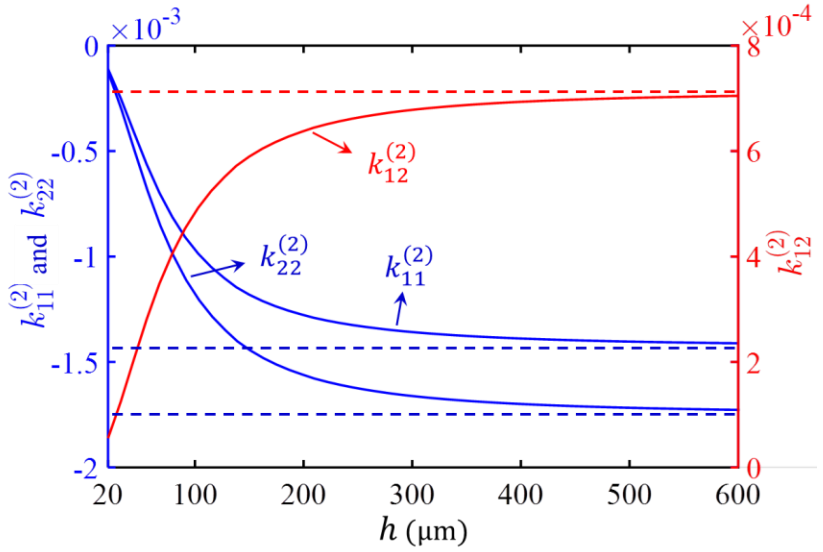

Fig. 4 Variations of the elements of the load stiffening matrix $\left[k_{ij}^{(1)}\right]$ of a strain gradient beam with h (dashed asymptotes are the corresponded results of the BCM model)

Considering Figs. 2-4, it is reasonable to expect the classical theory to provide erroneous predictions for the deflection of nano/micro flexure beams under the effect of end loads. To investigate this, a group of microbeams with specifications given in Table 4, but with $L/h = 20$ and $b/h = 2$ is considered. It is assumed that the beams are under the end transverse load of $F_Z = 100$ μN. In Fig. 5, the transverse deflection of such beams is depicted versus the thickness h, and the results obtained from the MSGBCM, classical and couple stress theories are compared. Moreover, to verify the accuracy of the proposed technique, the findings of the MSGBCM are also compared with those of Kong et al [48] whom used the modified strain gradient theory for their analysis, and an excellent agreement is observed. Fig. 5 shows that for the microbeams under study, when the thickness h is larger than 150 μm, all mentioned theories lead to almost the same deflections. However, at smaller scales, the approach of Kong et al [48] and MSGBCM predict smaller deflections for the system.

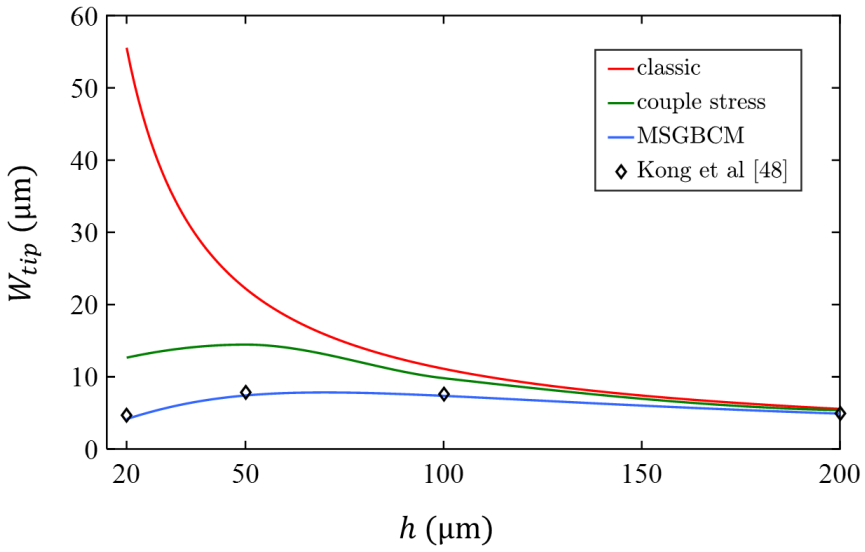

Fig. 5 Tip deflection of flexure microbeams versus beam thickness for a group of beams with specifications reported in Table 4 and with $L/h = 20$, $b/h = 2$ and $F_Z = 100$ μN

4- Application of MSGBCM to P-flexures

In this section, the load displacement formulation of a nano/micro-scale P-flexure will be presented. To this end, the P-flexure shown in Fig. 6 is considered.

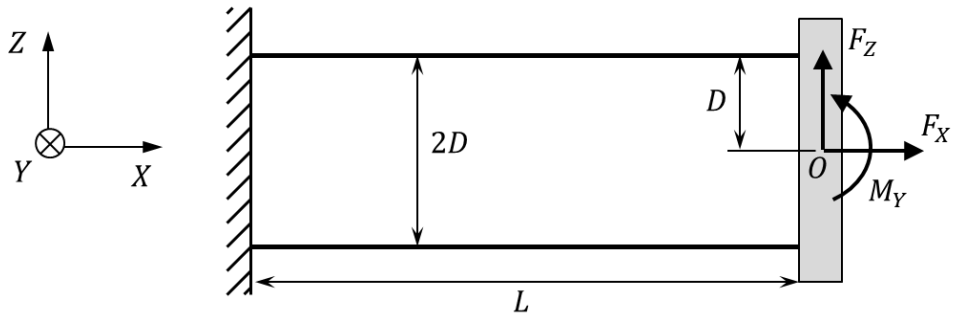

Fig. 6 Schematic view of the P-flexure under study

In the upcoming formulations, the upper and the lower beams of this figure are respectively denoted as the first and the second beams. Using geometrical relations, the dimensionless tip

displacements of the first and the second beams in Fig. 6 can be easily expressed in terms of axial (i.e. u_O) and transverse (i.e. w_O) dimensionless displacements of the point O as well as the rotation of the stage (i.e. θ_O) as

$$w_{tip}^{(i)} = w_O, \qquad i = 1,2 \tag{80}$$

$$\theta_{tip}^{(i)} = \theta_O, \qquad i = 1,2 \tag{81}$$

$$u_{tip}^{(i)} = u_O + (-1)^i (d)\theta_O, \qquad i = 1,2 \tag{82}$$

where in Eq. (82), $d = D/L$ is half of the normalized distance between the stage's center and the beams. Using Eq. (76), the strain energy of the i'th beam $v = v_i\left(w_{tip}^{(i)}, \theta_{tip}^{(i)}, u_{tip}^{(i)}\right)$ can be obtained. Then the total strain energy of the flexure is simply derived by

$$v = \sum_{i=1}^{2} v_i\left(w_{tip}^{(i)}, \theta_{tip}^{(i)}, u_{tip}^{(i)}\right) = \frac{1}{2}a_1 \frac{\sum_{i=1}^{2}\left(u_O + (-1)^i d\theta_O + \frac{1}{2}\{w_O \quad \theta_O\}\begin{bmatrix} k_{11}^{(1)} & k_{12}^{(1)} \\ k_{12}^{(1)} & k_{22}^{(1)} \end{bmatrix}\begin{Bmatrix} w_O \\ \theta_O \end{Bmatrix}\right)^2}{1 - a_1\{w_O \quad \theta_O\}\begin{bmatrix} k_{11}^{(2)} & k_{12}^{(2)} \\ k_{12}^{(2)} & k_{22}^{(2)} \end{bmatrix}\begin{Bmatrix} w_O \\ \theta_O \end{Bmatrix}}$$

$$+\{w_O \quad \theta_O\}\begin{bmatrix} k_{11}^{(0)} & k_{12}^{(0)} \\ k_{12}^{(0)} & k_{22}^{(0)} \end{bmatrix}\begin{Bmatrix} w_O \\ \theta_O \end{Bmatrix} \tag{83}$$

Using the virtual work principle $\tilde{\delta}v = f_x\tilde{\delta}u_O + f_z\tilde{\delta}w_O + m_y\tilde{\delta}\theta_O$, and employing Eq. (83), the load displacement relations for the nano/micro scale P-flexure is derived as

$$f_x = \frac{\partial v}{\partial u_O} = \frac{a_1\left(2u_O + k_{11}^{(1)}w_O^2 + 2k_{12}^{(1)}w_O\theta_O + k_{22}^{(1)}\theta_O^2\right)}{1 - a_1\left(k_{11}^{(2)}w_O^2 + 2k_{12}^{(2)}w_O\theta_O + k_{22}^{(2)}\theta_O^2\right)} \tag{84}$$

$$f_z = \frac{\partial v}{\partial w_O} = \frac{a_1\left(k_{11}^{(1)}w_O + k_{12}^{(1)}\theta_O\right)\left(2u_O + k_{11}^{(1)}w_O^2 + 2k_{12}^{(1)}w_O\theta_O + k_{22}^{(1)}\theta_O^2\right)}{1 - a_1\left(k_{11}^{(2)}w_O^2 + 2k_{12}^{(2)}w_O\theta_O + k_{22}^{(2)}\theta_O^2\right)}$$

$$+ \frac{1}{2}\frac{a_1^2\left(k_{11}^{(2)}w_O + k_{12}^{(2)}\theta_O\right)\left\{\left(2u_O + k_{11}^{(1)}w_O^2 + 2k_{12}^{(1)}w_O\theta_O + k_{22}^{(1)}\theta_O^2\right)^2 + 4d^2\theta_O^2\right\}}{\left(1 - a_1\left(k_{11}^{(2)}w_O^2 + 2k_{12}^{(2)}w_O\theta_O + k_{22}^{(2)}\theta_O^2\right)\right)^2}$$

$$+ 2\left(k_{11}^{(0)}w_O + k_{12}^{(0)}\theta_O\right) \tag{85}$$

$$m_y = \frac{\partial v}{\partial \theta_O} = \frac{a_1\left(k_{12}^{(1)}w_O + k_{22}^{(1)}\theta_O\right)\left(2u_O + k_{11}^{(1)}w_O^2 + 2k_{12}^{(1)}w_O\theta_O + k_{22}^{(1)}\theta_O^2\right) + 2a_1d^2\theta_O}{1 - a_1\left(k_{11}^{(2)}w_O^2 + 2k_{12}^{(2)}w_O\theta_O + k_{22}^{(2)}\theta_O^2\right)}$$

$$+ \frac{1}{2}\frac{a_1^2\left(k_{12}^{(2)}w_O + k_{22}^{(2)}\theta_O\right)\left\{\left(2u_O + k_{11}^{(1)}w_O^2 + 2k_{12}^{(1)}w_O\theta_O + k_{22}^{(1)}\theta_O^2\right)^2 + 4d^2\theta_O^2\right\}}{\left(1 - a_1\left(k_{11}^{(2)}w_O^2 + 2k_{12}^{(2)}w_O\theta_O + k_{22}^{(2)}\theta_O^2\right)\right)^2}$$

$$+ 2\left(k_{12}^{(0)}w_O + k_{22}^{(0)}\theta_O\right) \tag{86}$$

If the deflection of the flexure beams in P-flexure is smaller than $0.15L$, then comparing to w_O^2, the terms containing θ_O^2 and $w_O\theta_O$ can be ignored. By performing the mentioned simplifications, the load-displacement relationships are simplified as

$$f_x = a_1\left(\frac{2u_O + k_{11}^{(1)}w_O^2}{1 - a_1k_{11}^{(2)}w_O^2}\right) \tag{87}$$

$$f_z = 2\left(k_{11}^{(0)}w_O + k_{12}^{(0)}\theta_O\right) + \left(k_{11}^{(1)}w_O + k_{12}^{(1)}\theta_O\right)f_x + \frac{1}{2}\left(k_{11}^{(2)}w_O + k_{12}^{(2)}\theta_O\right)f_x^2 \tag{88}$$

$$m_y = 2\left(k_{12}^{(0)}w_O + k_{22}^{(0)}\theta_O\right) + \left(k_{12}^{(1)}w_O + k_{22}^{(1)}\theta_O\right)f_x + \frac{1}{2}\left(k_{12}^{(2)}w_O + k_{22}^{(2)}\theta_O\right)f_x^2$$

$$+ 2d^2\frac{a_1\theta_O}{1 - a_1k_{11}^{(2)}w_O^2} \tag{89}$$

To investigate the effect of axial and transverse load on end displacement components, a P-flexure with $h = 50$ μm and $D = 10h$ and with specifications reported in Table 4 is considered.

As sample simulations, the axial, transverse and rotational response of the flexure to a wide range of f_x and f_z have been illustrated in Figs. 7-9. For each load case, Eqs. (87)-(89) are numerically solved for (u_O, w_O, θ_O). As Fig. 7 suggests, at each f_x, the axial displacement of the stages center with f_z almost follows a parabolic shape. As physically expected, larger axial forces lead to smaller absolute axial displacements of the stage's center. Fig. 8 shows that transverse movement of the stage's center changes almost linearly with f_z. The slope of this linear relationship however is larger for smaller values of f_x. This indicate the physical expectation that when a compressive f_x is applied to the system, the system experiences larger transverse displacements with the same f_z. Finally, Fig. 9 shows that the variation of the rotation angle of the stage with f_z at different values of f_x, is very similar to the curve of a third order polynomial. Moreover, it is observed that the rotational angle of the stage of the micro scale P-flexure under study is very small (less than $0.15°$) in all simulated loading conditions.

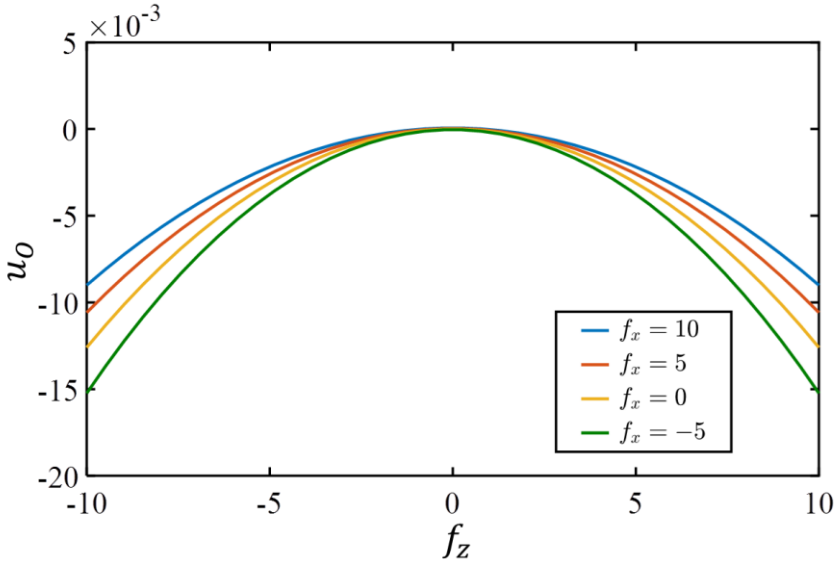

Fig. 7 Axial displacement of small-scale P-flexure versus transverse load at different axial forces

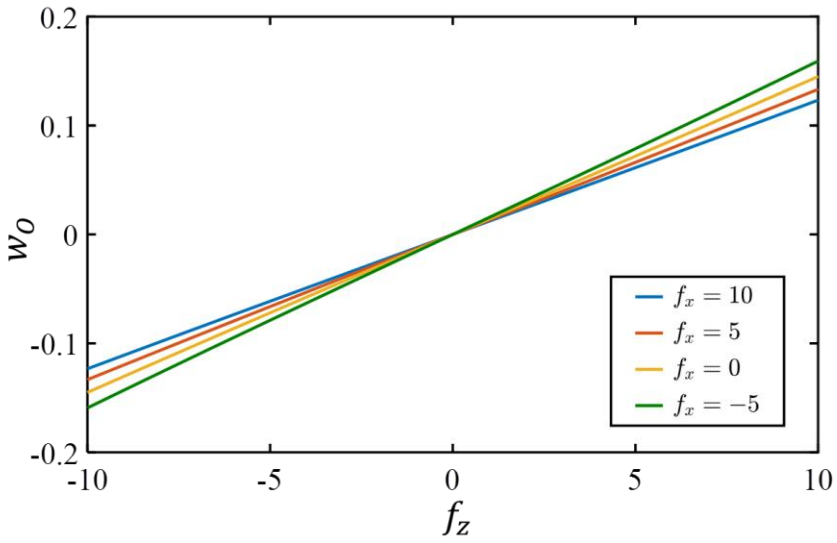

Fig. 8 Transverse displacement of small-scale P-flexure versus transverse load at different axial forces

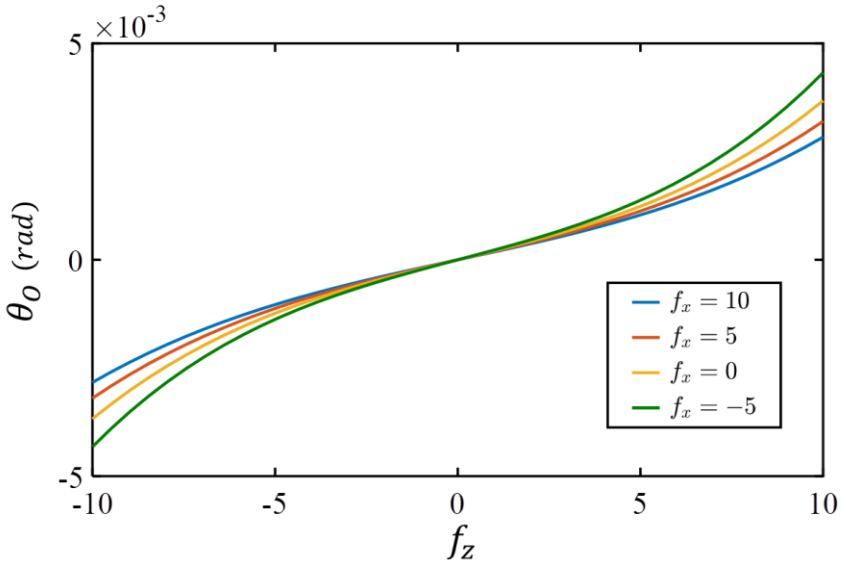

Fig. 9 Rotation of the motion stage of small-scale P-flexure versus transverse load at different axial forces

The load displacement equations (87)-(89) can be utilized for deriving the stiffnesses of the micro scale P-flexure. These directional stiffnesses can be easily derived by

$$k_x = \frac{\partial f_x(u_O, w_O)}{\partial u_O} = \frac{2a_1}{1 - a_1 k_{11}^{(2)} w_O^2} \tag{90}$$

$$k_z = \frac{\partial f_z(u_O, w_O, \theta_O)}{\partial w_O} = 2k_{11}^{(0)} + k_{11}^{(1)} f_x + \frac{1}{2} k_{11}^{(2)} f_x^2 \tag{91}$$

$$k_\theta = \frac{\partial m_y(u_O, w_O, \theta_O)}{\partial \theta_O} = 2k_{12}^{(0)} + k_{12}^{(1)} f_x + \frac{1}{2} k_{12}^{(2)} f_x^2 + 2d^2 \frac{a_1}{1 - a_1 k_{11}^{(2)} w_O^2} \tag{92}$$

To compare the results of the MSGBCM formulation with those of the BCM, some P flexures with $D = 10h$ and beam specifications given in Table 4 is considered. It is assumed that the flexure deflects solely under the effect of f_z. In Figs. 10-12, the stiffnesses k_x, k_z and k_θ versus w_O resulted from both BCM and MSGBCM formulations have been compared. As it is observed for the case of relatively larger h of 200 μm, both MSGBCM and BCM provides almost similar predictions for the stiffness of the flexure. However, for smaller sizes of the flexure such as $h = 50$ μm, the MSGBCM predicts larger stiffnesses. This result is especially interesting for design of compliant mechanisms which severely suffer from constraint direction stiffness loss as the motion stage moves in the DoF direction. In these cases, the results of the MSGBCM suggests that the mentioned stiffness loss is not as critical as predicted by a classical theory. As a result, the design process of such micro scale mechanisms can be carried out with much more flexibility in choosing the physical and geometrical specifications of the constituent material.

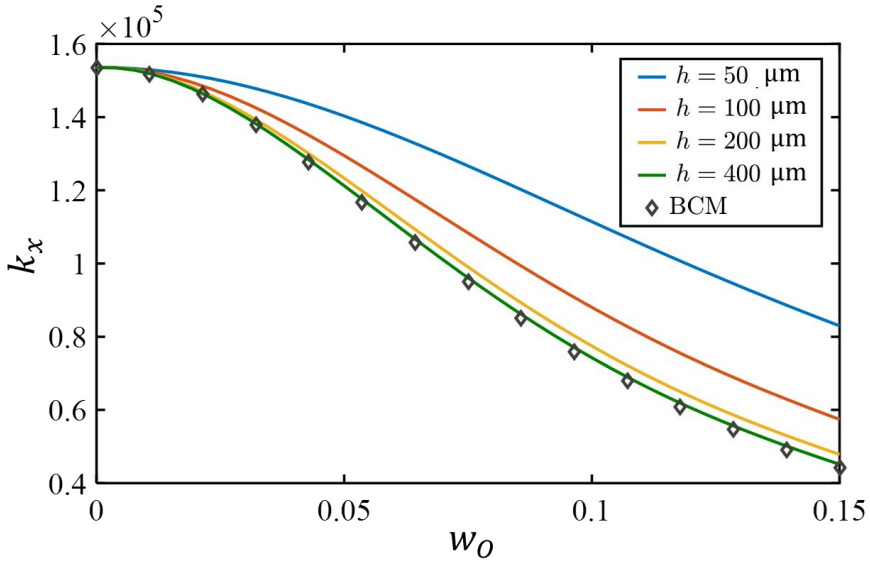

Fig. 10 Axial stiffness drop of a small-scale P-flexure versus w_o

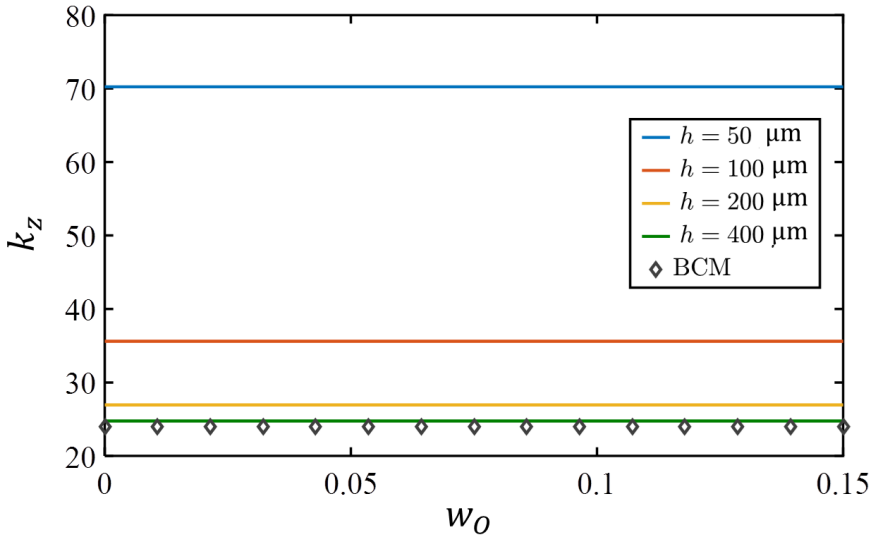

Fig. 11 Transverse stiffness of a small-scale P-flexure versus w_o

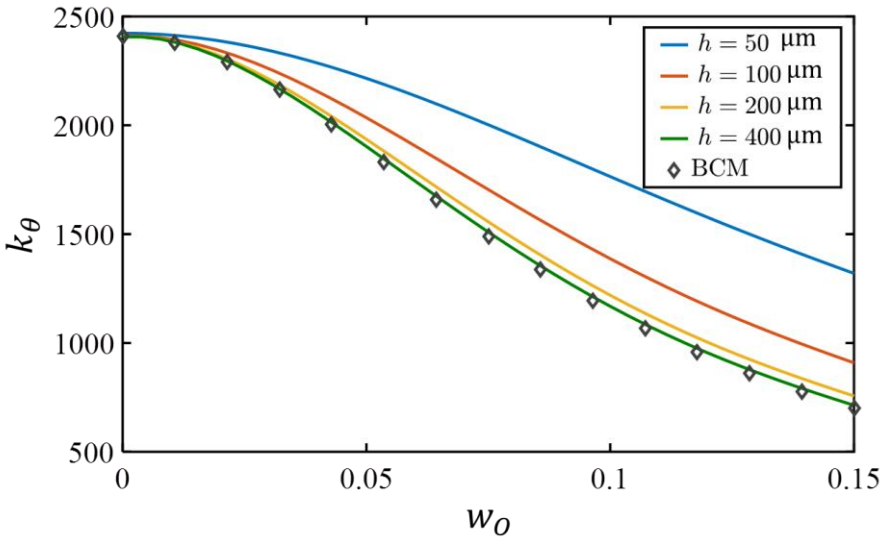

Fig. 12 Rotational stiffness of a small-scale P-flexure versus $\boldsymbol{w_o}$

5- Conclusion

Powerful techniques are available for design and analysis of macro scale flexure systems. However, these tools may not be sufficiently accurate for the design of nano or micro scale flexures. On the other hand, in small scales, flexure mechanisms may be the only solution for providing highly precise motion guidance. So, the importance of proposing new formulations capable of capturing small-scale effects in compliant units is well recognized. In this paper, a novel technique called MSGBCM was presented which utilized the modified strain gradient theory to amend BCM by enabling it to capture small scale effects. First, nonlinear strain energy expressions were presented for nano and micro scale beam flexures. Then the problem was formulated using the principle of the virtual work. The resulting equations were solved using the perturbation theory and closed-form expressions were presented for the load-displacement behavior of the system. Moreover, an analytic formula was presented for the nonlinear strain energy of the flexure beam

solely in terms of the length scales of the beam's material as well as its tip displacements. This energy expression was utilized to formulate the load-displacement behavior of micron and submicron size P-flexures. Overally, the obtained results clearly indicated that the behavior of flexure systems under end load conditions severely depends on h/l_i as a measure of the size of the structure. If the structure is large enough, then even the BCM can provide accurate prediction for the behavior of the flexure. Otherwise, the previously reported BCM may underestimate the stiffness of the structure. The methodology and the results presented in this paper can be easily extended for accurate modeling of more complex micron and submicron size compliant modules such as DP or DP-DP. This will enable design of new flexures with extended stable travel range.

Appendix I: Definition of the functions $\xi_{j,i}(x)$

The functions $\xi_{j,i}(x)$ are defined by

$$\xi_{j,i}(x) = \frac{\varrho_{j,i}(x)}{\zeta_{j,i}(x)}, \quad j = 1,2, \;\; i = 0,1,2 \tag{I-1}$$

where

$$\begin{aligned}\varrho_{1,0}(x) = {} & -12(b_1+1)e^{b_1(x-1)} - 6(b_1^2-2)e^{-b_1(x-2)} + 12(b_1-1)e^{b_1(x+1)} \\ & +(-x^2(2x-3)b_1^4 + 2x(x^2-3)b_1^3 - 6(x^2-1)b_1^2 + 12b_1x - 12)e^{2b_1} \\ & -6(b_1^2-2)e^{b_1x} + 12(x(x-2)b_1^2+3)e^{b_1} - (2x-3)x^2b_1^4 - 2x(x^2-3)b_1^3 \\ & -6(x^2-1)b_1^2 - 12(b_1x+1)\end{aligned} \tag{I-2}$$

$$\zeta_{1,0}(x) = (b_1^4 - 4b_1^3 + 24b_1 - 24)e^{2b_1} + b_1^4 + 4b_1^3 - 24b_1^2e^{b_1} - 24b_1 + 48e^{b_1} - 24 \tag{I-3}$$

$$\begin{aligned}\varrho_{2,0}(x) = {} & 6(b_1^2+2b_1+2)e^{-b_1(x-1)} + 2(b_1^3-6)e^{-b_1(x-2)} - 6(b_1^2-2b_1+2)e^{b_1(x+1)} \\ & +\left(x^2(x-1)b_1^5 + 2x(-x^2+1)b_1^4 + (2x^3-2)b_1^3 + 6(b_1^2x^2 - 2b_1x + 2)\right)e^{2b_1}\end{aligned} \tag{I-4}$$

$$+2(b_1^3+6)e^{b_1x}-4(x(x^2+3x-3)b_1^2-6x+6)b_1e^{b_1}+x^2(x-1){b_1}^5$$

$$+2x(x^2-1)b_1^4+2(x^3-1)b_1^2-6(b_1^2x^2+2b_1x+2)$$

$$\zeta_{2,0}(x)=b_1\left((b_1^4-4b_1^3+24b_1-24)e^{2b_1}+b_1^4+4b_1^3-24e^{b_1}b_1^2-24b_1+48e^{b_1}-24\right) \quad \text{(I-5)}$$

$$\varrho_{j,i}(x)=\{6(b_1^2-2)e^{b_1(-1+x)}+(0.5b_1^4+2b_1^3)e^{-b_1x}-12+x(x-1)^2b_1^5-2(x^3-3x^2+2)b_1^3$$

$$-6(x^2-2x)b_1^2-12(x-1)b_1+\Big(\big((2x^3-3x^2)b_1^4+2(x^3-3x)b_1^3+6(x^2-1)b_1^2$$

$$+12b_1x+12\big)e^{-b_1}+\big(-0.5b_1^4+2b_1^3-12b_1+12\big)e^{b_1x}\}\mathbb{I}_1^{(j,i)}$$

$$+2b_1\{3(b_1^2-2)e^{-b_1(x-1)}+3(b_1^2-2)e^{b_1(x-1)}+6(b_1+1)e^{-b_1x}$$

$$+\big(6+x^2(x-1.5)b_1^4+(x^3-3x)b_1^3+3(x^2-1)b_1^2+6b_1x\big)e^{-b_1}$$

$$+\big(6+x^2(x-1.5)b_1^4-(x^3-3x)b_1^3+3(x^2-1)b_1^2-6b_1x\big)e^{b_1}$$

$$-6(b_1-1)e^{b_1x}-12-6(x^2+2x)b_1^2\}\mathbb{I}_2^{(j,i)}$$

$$+\{2(b_1^3-6)e^{-b_1(x-1)}+2(b_1^3+6)e^{b_1(x-1)}+6(b_1^2+2b_1+2)e^{-b_1x}$$

$$+(-12+x^2(-1+x)b_1^5+2(x^3-x)b_1^4+2(x^3-1)b_1^3-6x^2b_1^2-12b_1x\big)e^{-b_1}$$

$$+\big(x^2(x-1)b_1^5-2(x^3-x)b_1^4+2(x^3-1)b_1^3+6x^2b_1^2-12b_1x+12\big)e^{b_1}$$

$$-6\big({b_1}^2-2b_1+2\big)e^{b_1x}-4b_1\left((x^3+3x^2-3x)b_1^2-6x+6\right)\Big\}\mathbb{I}_3^{(j,i)},\ \ j,i=1,2 \quad \text{(I-6)}$$

$$\zeta_{j,i}(x)=2b_2b_1^3\left(\left(b_1^4-24\right)\cosh(b_1)-4\left(b_1^3+6b_1\right)\sinh(b_1)-12b_1^2+24\right),\ \ j,i=1,2 \quad \text{(I-7)}$$

In Eq. (I-6), the parameters $\mathbb{I}_k^{(j,i)}$s are defined by

$$\mathbb{I}_1^{(j,i)}=\int_0^1 \xi_{j,i-1}(x)e^{-b_1(x-1)}dx \quad \text{(I-8)}$$

$$\mathbb{I}_2^{(j,i)}=\int_0^1 (x-1)\xi_{j,i-1}(x)dx \quad \text{(I-9)}$$

$$\mathbb{I}_3^{(j,i)}=\int_0^1 \xi_{j,i-1}(x)dx \quad \text{(I-10)}$$

References

[1] M. B. Akbarzadeh, H. Moeenfard, and S. Awtar, "Nonlinear dynamic modeling of a parallelogram flexure," *Mechanism and Machine Theory,* vol. 153, p. 103985, 2020.

[2] S. Wu, Z. Shao, H. Su, and H. Fu, "An energy-based approach for kinetostatic modeling of general compliant mechanisms," *Mechanism and Machine Theory,* vol. 142, p. 103588, 2019.

[3] F. Wang, B. Shi, Z. Huo, Y. Tian, and D. Zhang, "Control and dynamic releasing method of a piezoelectric actuated microgripper," *Precision Engineering,* vol. 68, pp. 1-9, 2021.

[4] T. K. Das, B. Shirinzadeh, A. Al-Jodah, M. Ghafarian, and J. Pinskier, "Computational parametric analysis and experimental investigations of a compact flexure-based microgripper," *Precision Engineering,* vol. 66, pp. 363-373, 2020.

[5] A. Bagolini, S. Ronchin, P. Bellutti, M. Chistè, M. Verotti, and N. P. Belfiore, "Fabrication of novel MEMS microgrippers by deep reactive ion etching with metal hard mask," *Journal of Microelectromechanical Systems,* vol. 26, pp. 926-934, 2017.

[6] A. Gawlik, W. Harmatys, S. Łaczek, and G. Tora, "Manipulator effecting 2D microdisplacements," in *IFToMM World Congress on Mechanism and Machine Science,* 2019, pp. 1829-1838.

[7] H. Li and G. Hao, "Position-space-based design of a symmetric spatial translational compliant mechanism for micro-/nano-manipulation," *Micromachines,* vol. 9, p. 189, 2018.

[8] M. T. Ahmadian and H. Jafarishad, "Design and analysis of a 3-link micro-manipulator actuated by piezoelectric layers," *Mechanism and Machine Theory,* vol. 112, pp. 43-60, 2017.

[9] S. Iqbal, R. I. Shakoor, Y. Lai, A. M. Malik, and S. A. Bazaz, "Experimental evaluation of force and amplification factor of three different variants of flexure based micro displacement amplification mechanism," *Microsystem Technologies*, vol. 25, pp. 2889-2906, 2019.

[10] Y.-J. Lei, R.-J. Li, R.-X. Chen, L.-S. Zhang, P.-H. Hu, Q.-X. Huang, *et al.*, "A high-precision two-dimensional micro-accelerometer for low-frequency and micro-vibrations," *Precision Engineering,* vol. 67, pp. 419-427, 2021.

[11] R.-J. Li, K.-C. Fan, Q.-X. Huang, H. Zhou, E.-M. Gong, and M. Xiang, "A long-stroke 3D contact scanning probe for micro/nano coordinate measuring machine," *Precision Engineering,* vol. 43, pp. 220-229, 2016.

[12] Y. Gao, C. Yan, H. Huang, T. Yang, G. Tian, D. Xiong, *et al.*, "Microchannel-Confined MXene Based Flexible Piezoresistive Multifunctional Micro-Force Sensor," *Advanced Functional Materials,* vol. 30, p. 1909603, 2020.

[13] H. Sadeghian, N. Koster, and T. van den Dool, "Introduction of a high throughput SPM for defect inspection and process control," in *Metrology, Inspection, and Process Control for Microlithography XXVII*, 2013, p. 868127.

[14] A. Mohammadi, A. G. Fowler, Y. K. Yong, and S. R. Moheimani, "A feedback controlled MEMS nanopositioner for on-chip high-speed AFM," *Journal of microelectromechanical systems,* vol. 23, pp. 610-619, 2013.

[15] A. Zhang and G. Chen, "A comprehensive elliptic integral solution to the large deflection problems of thin beams in compliant mechanisms," *Journal of Mechanisms and Robotics,* vol. 5, 2013.

[16] L. L. Howell, S. P. Magleby, and B. M. Olsen, *Handbook of compliant mechanisms*: John Wiley & Sons, 2013.

[17] V. K. Venkiteswaran and H.-J. Su, "A parameter optimization framework for determining the pseudo-rigid-body model of cantilever-beams," *Precision Engineering,* vol. 40, pp. 46-54, 2015.
[18] V. Mahesh, "Nonlinear deflection of carbon nanotube reinforced multiphase magneto-electro-elastic plates in thermal environment considering pyrocoupling effects," *Mathematical Methods in the Applied Sciences,* 2020.
[19] N. Anjum and J. H. He, "Nonlinear dynamic analysis of vibratory behavior of a graphene nano/microelectromechanical system," *Mathematical Methods in the Applied Sciences,* 2020.
[20] H. Moeenfard and S. Awtar, "Modeling geometric nonlinearities in the free vibration of a planar beam flexure with a tip mass," *Journal of Mechanical Design,* vol. 136, 2014.
[21] A. Koochi, M. Goharimanesh, and M. R. Gharib, "Nonlocal electromagnetic instability of carbon nanotube-based nano-sensor," Mathematical Methods in the Applied Sciences, 2021.
[22] S. Awtar and S. Sen, "A generalized constraint model for two-dimensional beam flexures: Nonlinear strain energy formulation," *Journal of mechanical Design,* vol. 132, 2010.
[23] M. Radgolchin and H. Moeenfard, "A constraint model for beam flexure modules with an intermediate semi-rigid element," *International Journal of Mechanical Sciences,* vol. 122, pp. 167-183, 2017.
[24] M. Bakhtiari-Shahri and H. Moeenfard, "Topology optimization of fundamental compliant mechanisms using a novel asymmetric beam flexure," *International Journal of Mechanical Sciences,* vol. 135, pp. 383-397, 2018.
[25] H. Malaeke and H. Moeenfard, "A novel flexure beam module with low stiffness loss in compliant mechanisms," *Precision Engineering,* vol. 48, pp. 216-233, 2017.
[26] R. M. Panas and J. B. Hopkins, "Eliminating underconstraint in double parallelogram flexure mechanisms," *Journal of mechanical Design,* vol. 137, 2015.
[27] M. Radgolchin and H. Moeenfard, "Load-displacement behavior of fundamental flexure modules interconnected with compliant elements," *Mechanism and Machine Theory,* vol. 120, pp. 120-139, 2018.
[28] N. B. Hubbard, J. W. Wittwer, J. A. Kennedy, D. L. Wilcox, and L. L. Howell, "A novel fully compliant planar linear-motion mechanism," in *ASME 2004 International Design Engineering Technical Conferences and Computers and Information in Engineering Conference*, 2004, pp. 1-5.
[29] L. Cui, C. Okwudire, and S. Awtar, "Modeling complex nonminimum phase zeros in flexure mechanisms," *Journal of Dynamic Systems, Measurement, and Control,* vol. 139, 2017.
[30] L. Cui and S. Awtar, "Experimental validation of complex non-minimum phase zeros in a flexure mechanism," *Precision Engineering,* vol. 60, pp. 167-177, 2019.
[31] M. Olfatnia, S. Sood, and S. Awtar, "Note: An asymmetric flexure mechanism for comb-drive actuators," *Review of Scientific Instruments,* vol. 83, p. 116105, 2012.
[32] M. Olfatnia, S. Sood, J. J. Gorman, and S. Awtar, "Large stroke electrostatic comb-drive actuators enabled by a novel flexure mechanism," *Journal of Microelectromechanical Systems,* vol. 22, pp. 483-494, 2012.
[33] M. Olfatnia, L. Cui, P. Chopra, and S. Awtar, "Large range dual-axis micro-stage driven by electrostatic comb-drive actuators," *Journal of Micromechanics and Microengineering,* vol. 23, p. 105008, 2013.

[34] D. C. Lam, F. Yang, A. Chong, J. Wang, and P. Tong, "Experiments and theory in strain gradient elasticity," *Journal of the Mechanics and Physics of Solids,* vol. 51, pp. 1477-1508, 2003.
[35] Q. Ma and D. R. Clarke, "Size dependent hardness of silver single crystals," *Journal of Materials Research,* vol. 10, pp. 853-863, 1995.
[36] A. W. McFarland and J. S. Colton, "Role of material microstructure in plate stiffness with relevance to microcantilever sensors," *Journal of Micromechanics and Microengineering,* vol. 15, p. 1060, 2005.
[37] J. S. Stölken and A. Evans, "A microbend test method for measuring the plasticity length scale," *Acta Materialia,* vol. 46, pp. 5109-5115, 1998.
[38] E. M. P. Cosserat, *Theory of deformable bodies*: National Aeronautics and Space Administration, 1970.
[39] R. Mindlin and H. Tiersten, "Effects of couple-stresses in linear elasticity," COLUMBIA UNIV NEW YORK1962.
[40] R. A. Toupin, "Elastic materials with couple-stresses," *Archive for Rational Mechanics and Analysis,* vol. 11, pp. 385-414, 1962.
[41] A. C. Eringen, "Theory of nonlocal thermoelasticity," *International Journal of Engineering Science,* vol. 12, pp. 1063-1077, 1974.
[42] F. Yang, A. Chong, D. C. C. Lam, and P. Tong, "Couple stress based strain gradient theory for elasticity," *International Journal of Solids and Structures,* vol. 39, pp. 2731-2743, 2002.
[43] B. Akgöz and Ö. Civalek, "Buckling analysis of cantilever carbon nanotubes using the strain gradient elasticity and modified couple stress theories," *Journal of Computational and Theoretical Nanoscience,* vol. 8, pp. 1821-1827, 2011.
[44] M. Z. Nejad and A. Hadi, "Eringen's non-local elasticity theory for bending analysis of bi-directional functionally graded Euler–Bernoulli nano-beams," *International Journal of Engineering Science,* vol. 106, pp. 1-9, 2016.
[45] Y. Li and M. Li, "Dynamic analysis of rotating double-tapered cantilever Timoshenko nano-beam using the nonlocal strain gradient theory," *Mathematical Methods in the Applied Sciences,* vol. 43, pp. 9206-9222, 2020.
[46] M. Radgolchin and H. Moeenfard, "Size-dependent nonlinear vibration analysis of shear deformable microarches using strain gradient theory," *Acta Mechanica,* vol. 229, pp. 3025-3049, 2018.
[47] R. Vatankhah and M. Kahrobaiyan, "Investigation of size-dependency in free-vibration of micro-resonators based on the strain gradient theory," *Latin American Journal of Solids and Structures,* vol. 13, pp. 498-515, 2016.
[48] S. Kong, S. Zhou, Z. Nie, and K. Wang, "Static and dynamic analysis of micro beams based on strain gradient elasticity theory," *International Journal of Engineering Science,* vol. 47, pp. 487-498, 2009.
[49] B. Wang, J. Zhao, and S. Zhou, "A micro scale Timoshenko beam model based on strain gradient elasticity theory," *European Journal of Mechanics-A/Solids,* vol. 29, pp. 591-599, 2010.
[50] M. Radgolchin and H. Moeenfard, "Size-dependent piezoelectric energy-harvesting analysis of micro/nano bridges subjected to random ambient excitations," *Smart Materials and Structures,* vol. 27, p. 025015, 2018.

[51] M. Kahrobaiyan, M. Asghari, M. Rahaeifard, and M. Ahmadian, "A nonlinear strain gradient beam formulation," *International Journal of Engineering Science*, vol. 49, pp. 1256-1267, 2011.
[52] M. Rahaeifard, M. Kahrobaiyan, M. Ahmadian, and K. Firoozbakhsh, "Size-dependent pull-in phenomena in nonlinear microbridges," *International Journal of Mechanical Sciences,* vol. 54, pp. 306-310, 2012.
[53] B. Akgöz and Ö. Civalek, "A new trigonometric beam model for buckling of strain gradient microbeams," *International Journal of Mechanical Sciences,* vol. 81, pp. 88-94, 2014.
[54] A. Lazopoulos, K. Lazopoulos, and G. Palassopoulos, "Nonlinear bending and buckling for strain gradient elastic beams," *Applied Mathematical Modelling,* vol. 38, pp. 253-262, 2014.
[55] S. S. Rao, *Vibration of continuous systems* vol. 464: Wiley Online Library, 2007.
[56] J. N. Reddy, *Theory and analysis of elastic plates and shells*: CRC press, 2006.
[57] J. Zhao, S. Zhou, B. Wang, and X. Wang, "Nonlinear microbeam model based on strain gradient theory," *Applied Mathematical Modelling,* vol. 36, pp. 2674-2686, 2012.
[58] E. Russell Johnston, *Mechanics of materials*: Copyright, 2012.